Finite Element Analysis of Thermoplastic Melts Flow through the Metering and Die Regions of Single Screw Extruders

M. H. R. GHOREISHY, M. RAZAVI NOURI

Polymer Research Center of Iran, P. O. Box 14185-458, Tehran, Iran

Received 23 September 1998; accepted 9 February 1999

ABSTRACT: This research work is devoted to the development of a mathematical model for the simulation of the flow of polymer melts through the metering and die regions of single screw extruders. The sets of the governing equations (flow and energy) are solved using the finite element method. The power-law model is used to describe the non-Newtonian rheological behavior of the fluid. The standard Galerkin technique is used in conjunction with the continuous penalty scheme to solve the flow equations. Due to the low thermal diffusivity of the polymer melts, a streamline upwinding Petrov–Galerkin method is used to obtain convergent and stable results for the energy equation. This method is based on the extension of a previously developed scheme. The overall solution strategy is based on the Picard iterative scheme. Simulation results are obtained for the flow of a polypropylene melt through the metering and die zones of a laboratory scale extruder. To validate the proposed model, the results of the computer simulations are compared with experimentally measured mass flow rate and pressure profile. These comparisons show that there is very good agreement between the model predictions and actual data. © 1999 John Wiley & Sons, Inc. J Appl Polym Sci 74: 676–689, 1999

Key words: extrusion; finite element; die; metering; power-law; polypropylene

INTRODUCTION

Single screw extrusion is one of the most important fabrication operations used in plastics and rubber industries. It is defined as a continuous process in which polymeric materials are changed to a viscous form, pumped and pressurized using a screw, and shaped to final form. It is a standard operation in the polymer processing field, and is widely used for many products such as profiles, fibers, strips, films, etc. It is also employed in a variety of manufacturing techniques, for example, injection and blow moldings. The development of a superior design for the screw and die, and also the optimization of the process, would enable more efficient use of raw materials and energy. For the screw, the most important parameters that should be taken into consideration during the design of the channel geometry are (i) generation of a uniform pressure and temperature distribution throughout the screw and (ii) elimination the possibilities of occurring stagnation points and partially filled regions. On the other hand, the design of extrusion dies is mainly determined by the required extrudate cross-sectional shape. In addition to the above mentioned parameters, efforts are normally made (i) to establish a streamlined flow pattern in the flow domain, (i) to generate an optimum pressure profile consistent with screw system, and (iii) to keep the die swell as low as possible. These tasks may be best achieved by developing a robust mathe-

Correspondence to: M. H. R. Ghoreishy.

Journal of Applied Polymer Science, Vol. 74, 676–689 (1999)
 CCC 0021-8995/99/030676-14

matical model based on physical law and assumptions to predict the flow field behavior in response to the changes of the domain geometries and process conditions. A detailed literature survey indicates that over the last three decades, mathematical modeling of the extrusion process and specifically the flow in the metering and die zones have been frequently studied with varying degrees of complexities.[1–15] The quantitative description of the flow of polymer melts in the screw channel and die requires consideration of sophisticated parameters, such as the non-Newtonian rheological behavior of polymer melts, complex three-dimensional flow patterns, nonisothermal condition established inside the flow domain, as well as the intricate boundary conditions. Consequently, most of the attempts have been concentrated on developing simplified models that normally give approximate results. Comparisons between the experimental data and the results of such models show that there is generally an error level about 10–20% between the calculated and measured mass flow rates.[8] The apparent discrepancies between the experiments and simulations can be attributed to some of the unreasonable simplifying assumptions that are normally made in the development of the mathematical models for the simulation of polymer melts flow through the melt conveying and die regions. The most important neglected features of the melt flow in single screw extruder are the three-dimensional flow regime and complex heat transfer process that takes place inside the channel and die systems. Moreover, using the simplified numerical methods or analytical techniques for the solution of the governing equations further reduce the general applicability of these models.

The aim of the present work is to develop a mathematical model for the simulation of the flow of polymer melts through the metering and die regions of single screw extruders. This model can be used not only to study the effects of various process conditions and geometry variations on the performance of the process but also to predict the operating point of the extruder machine. In addition, in order to investigate the capability of the developed model, the results of the simulations are compared with experimental data. The main assumptions made in the development of this model follows:

1. The flow regime of the polymer is laminar and steady state, and the fluid is incompressible.
2. The rheological behavior of the polymer melt is considered to be described by the power-law model.

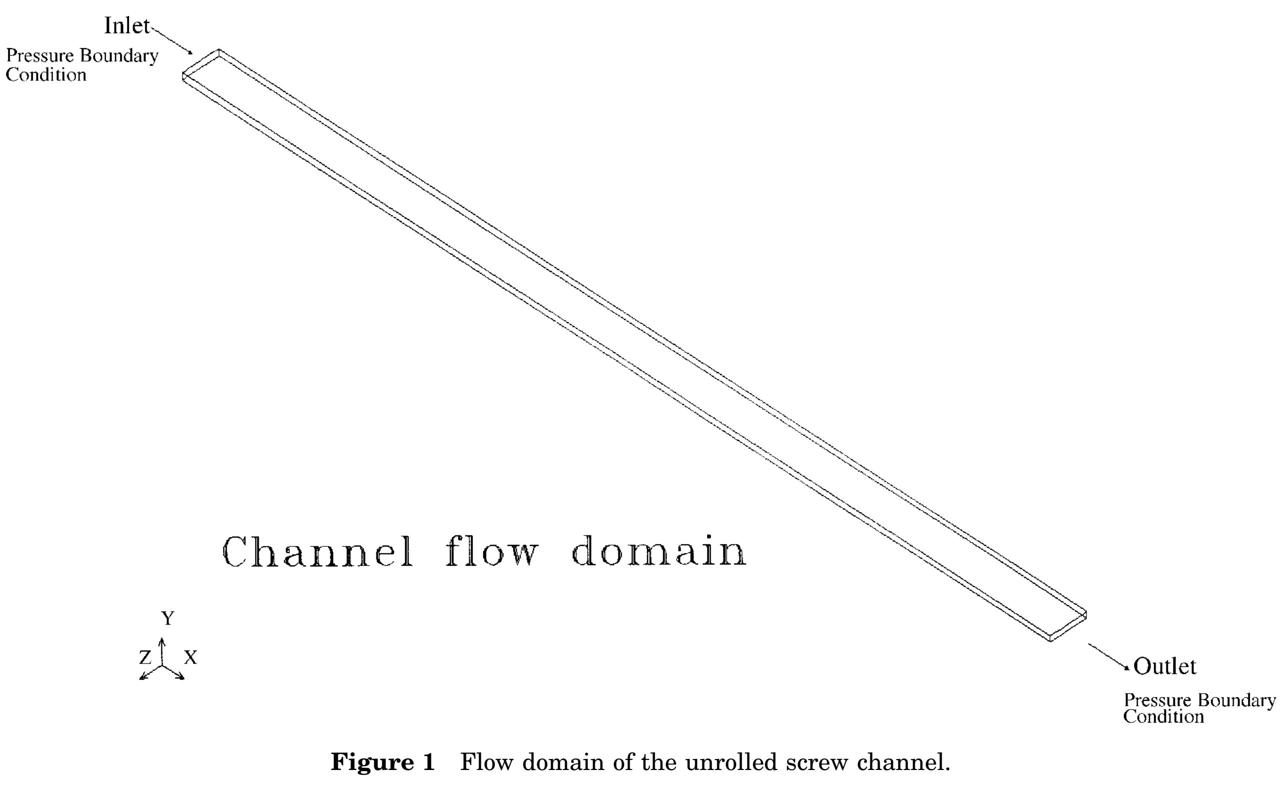

Figure 1 Flow domain of the unrolled screw channel.

3. There is no slip of the polymer melt on the solid boundaries.
4. The screw is assumed to be fixed within a rotating barrel and the channel is unrolled as a rectangular domain.

It can be seen that except for the fourth assumption, no limitation is associated with this problem. Therefore, the present model not only can effectively cope with the flow in single screw extruders but it offers a general method to any other flow problems encountered in polymer processing. It should be noted that although this model does not include the melting and solid conveying zones, it can be easily integrated with the previously developed models (see, for example, refs. 3–5 and 16) of these zones and thus uses the results of them as boundary conditions.

In the following sections, we first describe the mathematical model and then introduce the finite element formulations associated with this problem. The results of the computer simulation for the flow of a polypropylene melt (T30S) through the metering and die regions of a Haake–Buchler 19.05 mm (0.75 in.) single screw extruder are presented in the next section. These results are compared with measured pressure profile along the flow domain and output mass flow rates. It is shown that there are good agreements between the model predictions and experimental data, which confirm the validity of the present model.

MATHEMATICAL MODEL

The governing equations of the steady-state, nonisothermal, and laminar flow of an incompressible non-Newtonian fluid in a three-dimensional Cartesian coordinate system are given as follows[17]:

—The continuity equation,

$$\nabla \cdot \mathbf{v} = 0 \tag{1}$$

—The flow equation,

$$\rho \frac{D\mathbf{v}}{Dt} = -\nabla p + \nabla \cdot \boldsymbol{\tau} + \rho \mathbf{g} \tag{2}$$

—The energy equation,

$$\rho C_p \frac{DT}{Dt} = \nabla \cdot (k \nabla T) + \boldsymbol{\tau} : \nabla \mathbf{v} \tag{3}$$

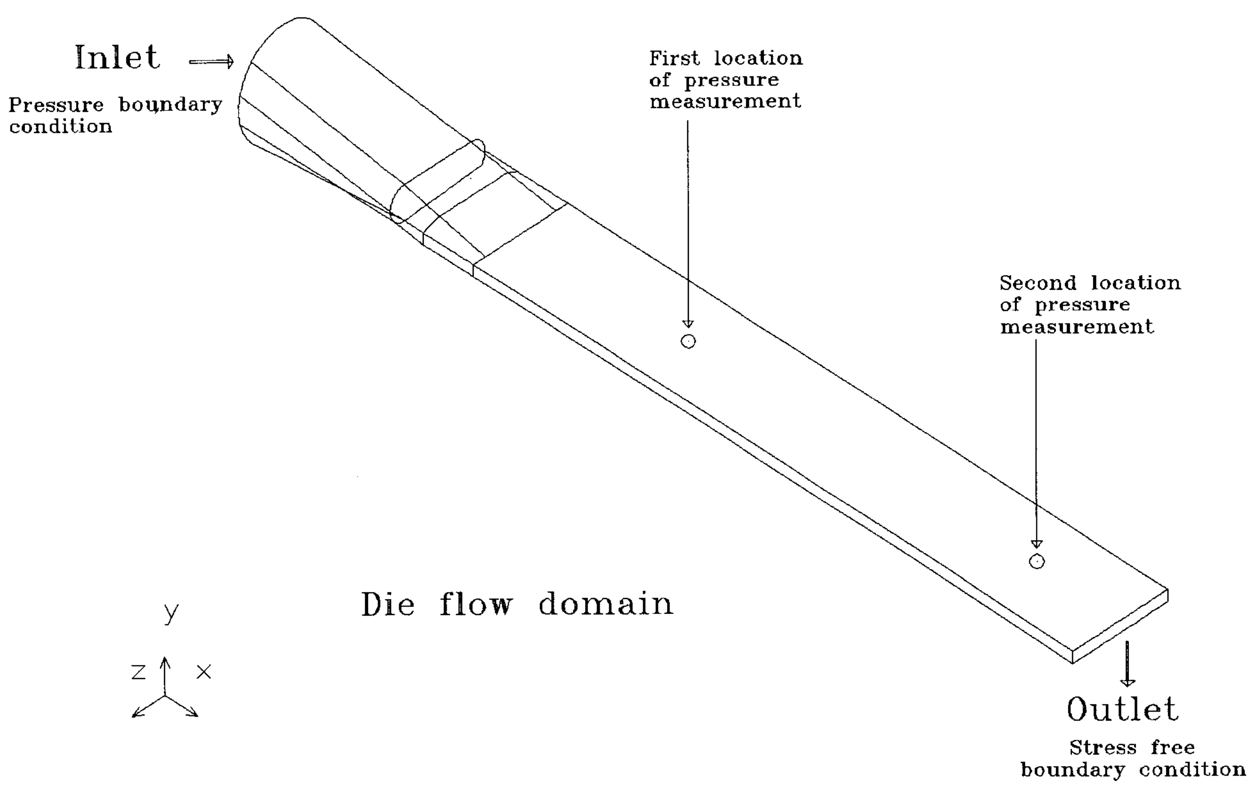

Figure 2 Flow domain of the die.

In these equations, $\mathbf{v}$ is the velocity vector, p is the pressure, ρ is the material density, $\mathbf{g}$ is the vector of gravity force per unit mass, T is the temperature, C_p is the heat capacity, and k is the thermal conductivity. Stress tensor $\boldsymbol{\tau}$ is given for a generalized Newtonian fluid in term of rate-of-deformation tensor $\boldsymbol{\Delta}$ by

$$\boldsymbol{\tau} = \eta \boldsymbol{\Delta} \tag{4}$$

where η is the shear dependent non-Newtonian viscosity of the fluid. The rate-of-deformation tensor is given as

$$\boldsymbol{\Delta} = \nabla \mathbf{v} + (\nabla \mathbf{v})^T \tag{5}$$

Viscosity η in the present study is given by the power-law equation expressed as

$$\eta = \eta_0 \left(\frac{1}{2} I_2 \right)^{(n-1)/2} e^{-b(T-T_R)} \tag{6}$$

where η_0 is the consistency of the fluid, n is the power-law index, T_R is a reference temperature, b is the temperature sensitivity factor, and I_2 is the second invariant of the rate-of-deformation tensor defined as

$$I_2 = \boldsymbol{\Delta} : \boldsymbol{\Delta} \tag{7}$$

FINITE ELEMENT FORMULATION

Flow Equations

The finite element formulation of the flow equations can be based on either a pressure-velocity

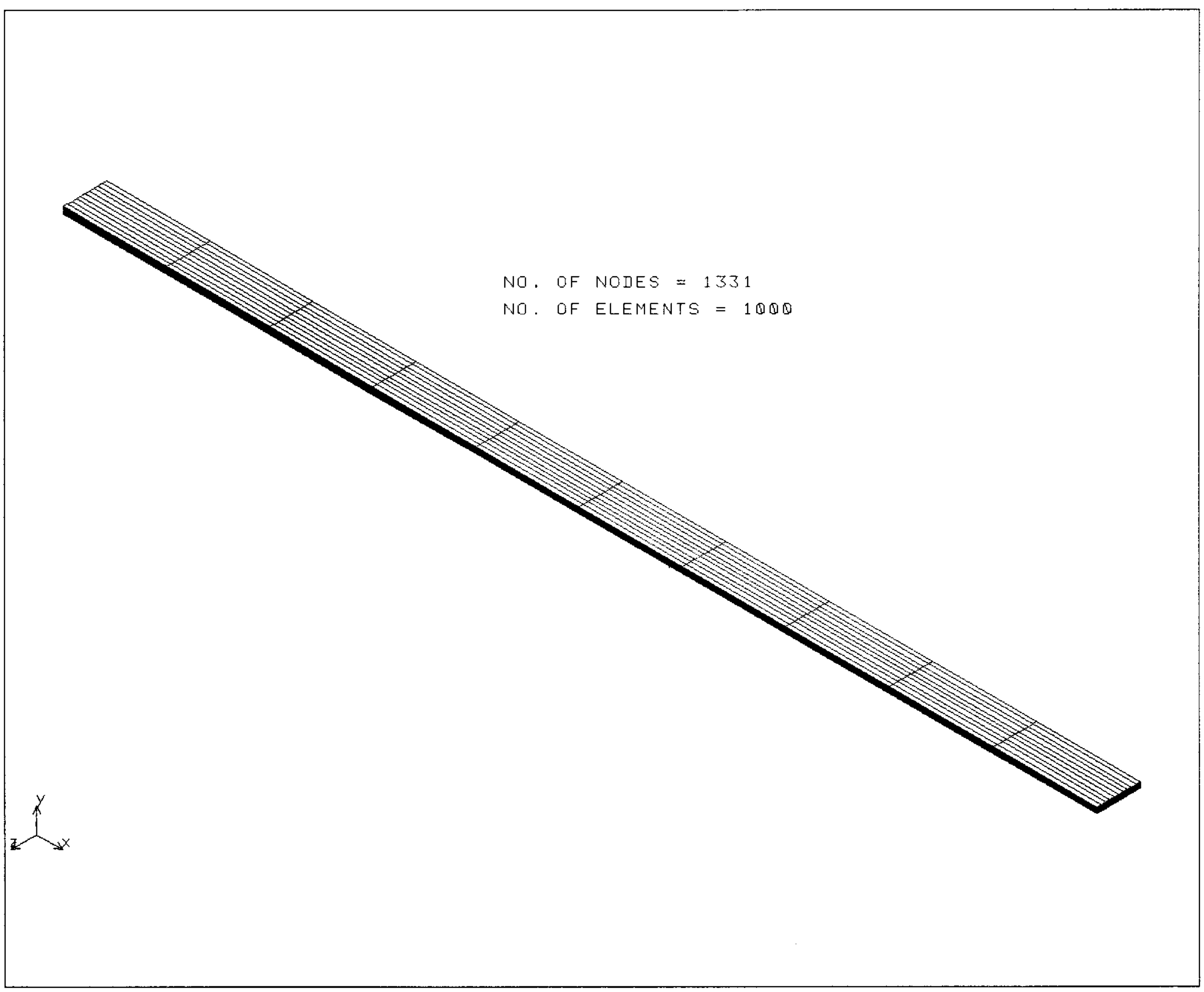

Figure 3 Finite element mesh of the screw channel.

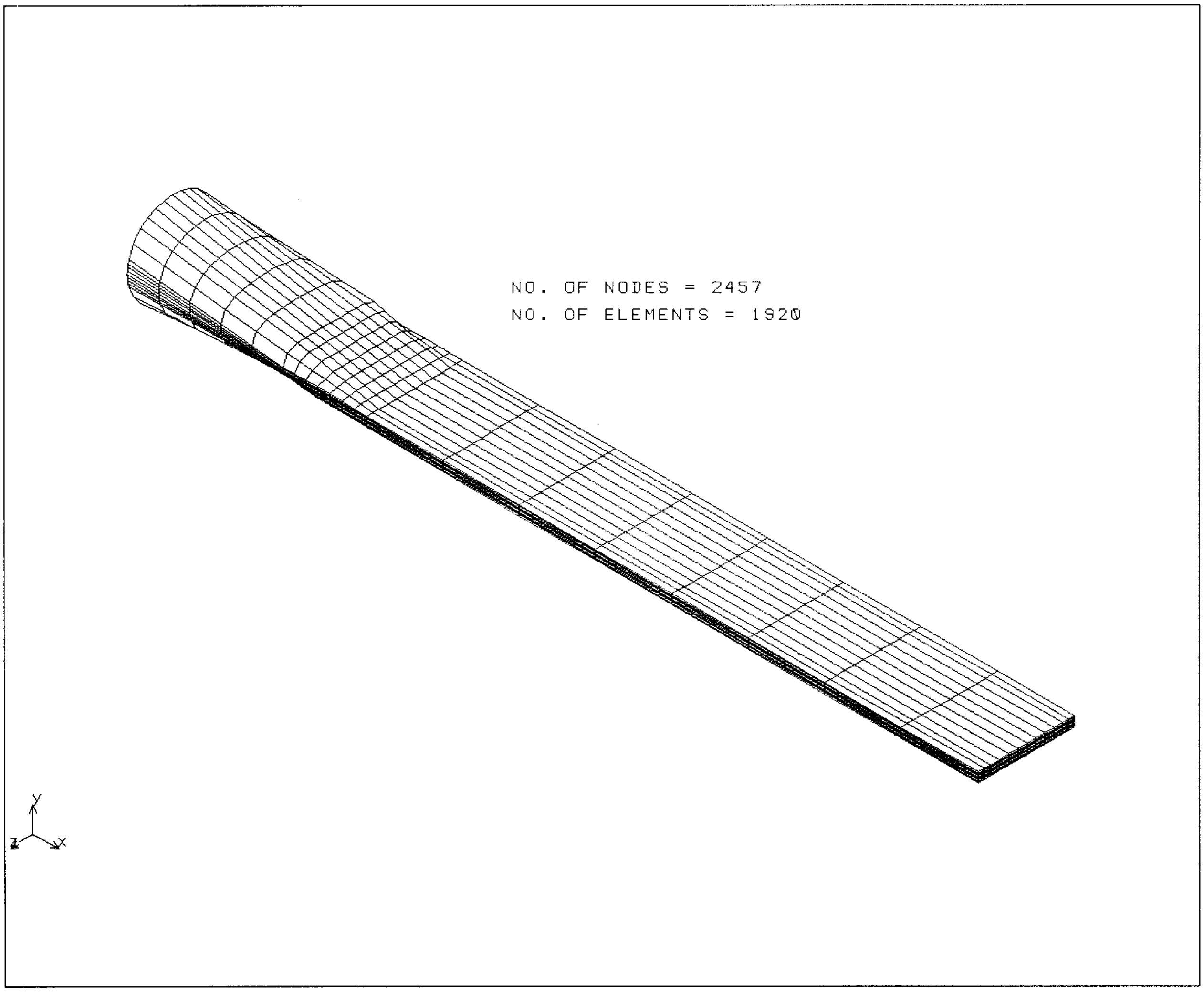

Figure 4 Finite element mesh of the die.

(called mixed or u-v-p) scheme or the use of penalty methods.[18] In the present study we have selected a penalty technique because these schemes produce a more compact set of working equations, thus reducing the required computer storage and computational cost. Furthermore, it is shown that for highly viscous fluids considered here, the penalty method gives more accurate solutions than the u-v-p method.[19]

The basic step in the penalty formulation is the elimination of the pressure term in momentum equations using

Table I Extruder Geometry and Dimensions

Parameter	Value
Barrel diameter (m)	0.019177
Screw diameter (m)	0.01905
Screw helix angle (deg)	17.66
Screw pitch (m)	0.01905
Axial length (m)	0.1077
Initial height (m)	0.002345
Final height (m)	0.001905
Channel width (m)	0.01498

Table II Properties of Polypropylene Melt

Power-law model	
Power-law index	0.5
Power-law constant (Pa-s^n)	6010
Reference temperature (°C)	200
Temperature sensitivity (°C^{-1})	0.0067
Physical properties	
Thermal conductivity (W/m°C)	0.1873
Density (kg/m^3)	749.6
Heat capacity (J/kg°C)	2428

$$p = -\lambda^*(\nabla \cdot \mathbf{v}) \tag{8}$$

where λ^* is a penalty parameter. It can be shown that if we choose λ^* to be a relatively large number, the continuity equation will be satisfied. It is recommended that the value of the λ^* be chosen as a function of viscosity to ensure uniform continuity enforcement in non-Newtonian problems.[18] Therefore equation λ^* is written as

$$\lambda^* = \eta\lambda \tag{9}$$

In this equation, η is the local viscosity and λ is a large constant positive number. This number is generally determined by numerical trial and error. In this work, it is found that a number of 10^{10} gives the most accurate results. Elimination of the pressure as a primary unknown by the penalty method can be achieved either by direct substitution of the pressure in the flow model using eq. (8) (continuous penalty method) or by using the discretized form of this equation to derive a set of compact working equations in the finite element scheme. The pressure field in these methods is found by a secondary calculation such as the variational recovery method.[20] In the present work we have used a continuous penalty technique since numerical experiments showed that this method gives a more accurate pressure field in our problem.

Following the procedures of weighted residual finite element schemes, the prime unknowns in

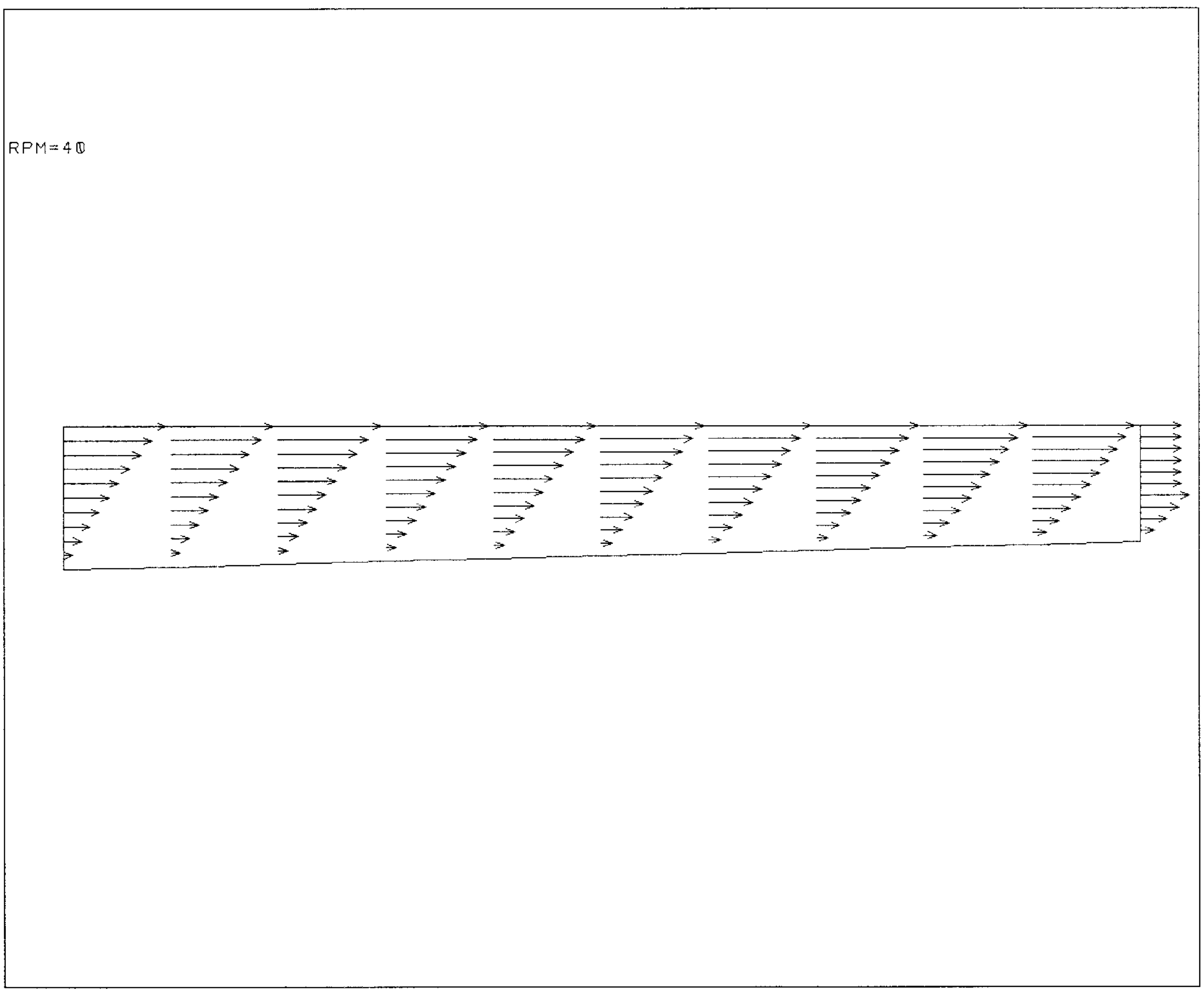

a

Figure 5 (a) Velocity in the down channel (x) direction (40 rpm). (b) Velocity field in cross channel (z) direction (40 rpm).

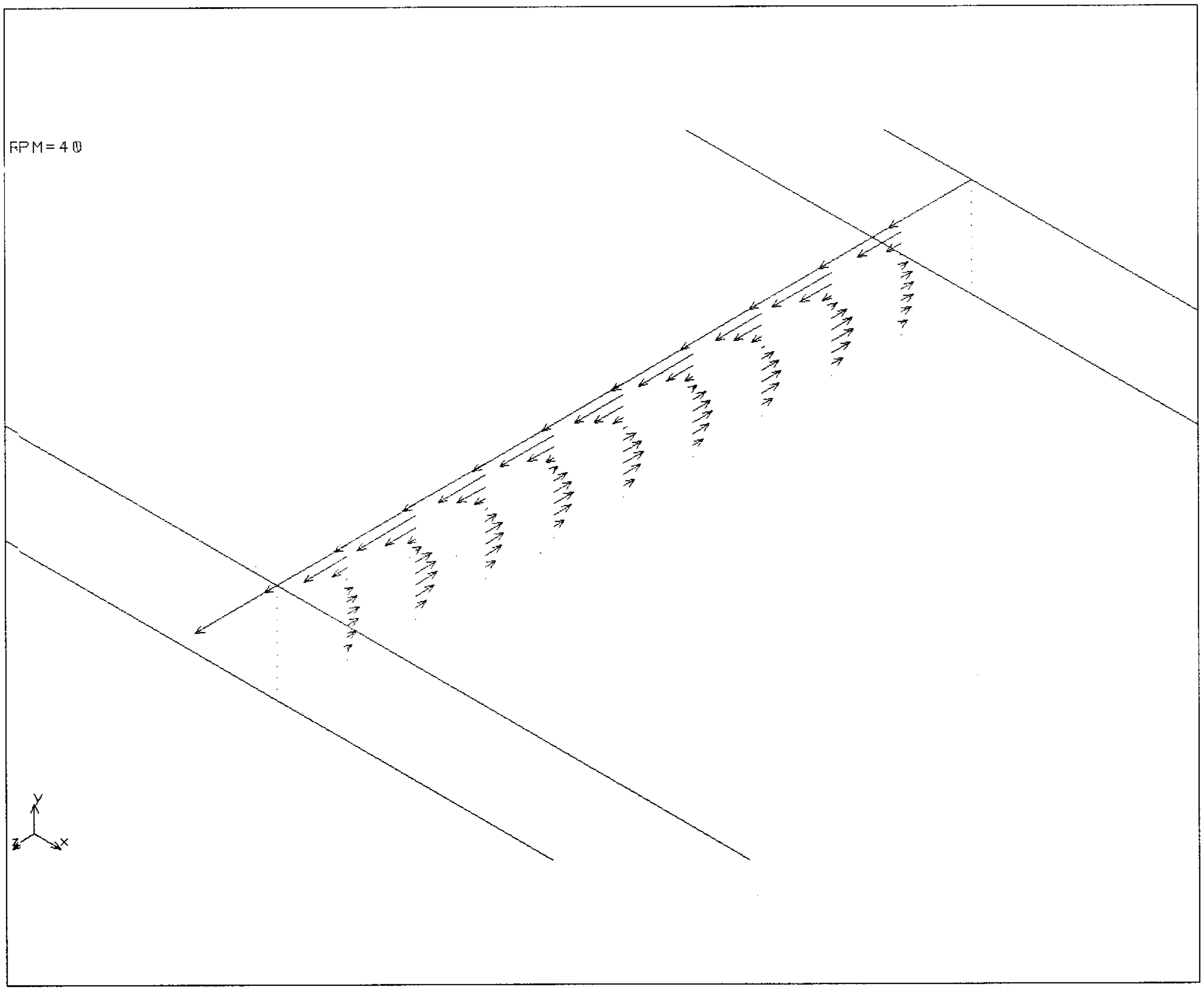

b

Figure 5 (*Continued from the previous page*)

the model are replaced by trial function representations that in the context of a discretized domain are given by polynomial relationships. This results in the derivation of basic residual statements of the scheme. These residuals are then multiplied by weight functions and their integrals over an element domain are set to be zero. Using the Galerkin method in which the weight and the interpolation functions are identical, the working flow equation of our scheme is derived as

$$[\mathbf{K}_\mathbf{f}^{(e)}]\{\mathbf{v}\} = \{\mathbf{F}_\mathbf{f}^{(e)}\} \tag{10}$$

where $\{\mathbf{v}\}$ is the vector of unknowns, $[\mathbf{K}_\mathbf{f}^{(e)}]$ and $\{\mathbf{F}_\mathbf{f}^{(e)}\}$ are the elemental stiffness and load vector, respectively [see appendix for the components of eq. (10)].

Energy Equation

Due to the low thermal conductivity of polymers, the main mechanism of heat transport in a flow regime involving these materials is convection. It is well known that the numerical simulation of convection-dominated transport phenomena by the standard Galerkin method gives unstable and oscillatory results. To eliminate such oscillations, in the present problem, we have used a streamline upwind Petrov–Galerkin technique. This method was originally developed by Brooks and Hughes[21] for two-dimensional problems. In the scheme used in our work, we have extended this technique for three-dimensional problems. The weight functions are described by the following relation:

$$W_i = \Psi_i + \frac{\Phi}{\|\mathbf{v}\|^2}(\mathbf{v}\cdot\nabla\Psi) \tag{11}$$

where W_i and ψ_i are the weight and interpolation functions, respectively, and Φ is a multiplier that in the present scheme is defined by

$$\Phi = \frac{\alpha_\xi h_\xi v_\xi + \alpha_\eta h_\eta v_\eta + \alpha_\zeta h_\zeta v_\zeta}{2} \tag{12}$$

where α_ξ, α_η and α_ζ are scalar parameters related to mesh Peclet number; h_ξ, h_η, and h_ζ are the element characteristic dimensions; and v_ξ, v_η, and v_ζ are the velocity components in the local elemental coordinate system ξ, η, and ζ, respectively. Similar to flow equations, the weighted residuals finite element method is used for energy equation. For the convection term, W_i is used while ψ_i (standard Galerkin) is applied to the other terms of eq. (3). Carrying out integration by parts and using of an appropriate interpolation relation for temperature, the finite element working equation corresponding to energy equation is derived as

$$[\mathbf{K}_\mathbf{v}^{(e)} + \mathbf{K}_\mathbf{d}^{(e)}]\{\mathbf{T}\} = \{\mathbf{F}_\mathbf{T}^{(e)}\} \tag{13}$$

where $\{\mathbf{T}\}$ is the vector of unknowns, $\mathbf{K}_\mathbf{v}^{(e)}$ and $\mathbf{K}_\mathbf{d}^{(e)}$ are the elemental convection and conduction stiffness matrices, respectively, and $\{\mathbf{F}_\mathbf{T}^{(e)}\}$ is the elemental load vector (see appendix).

In order to complete the mathematical model, the governing equations must be solved in conjunction with the appropriate sets of boundary conditions. The boundary conditions used in this work are as follows: On the solid walls the no-slip and constant temperature are used, which are the first type boundary conditions. For the inlet and outlet of the flow domains, pressure and stress free conditions (second type boundary conditions) are specified. It should be noted that the stress-free boundary condition is only used for the outlet section of the extrusion die. This is because that at the outlet, the material would be in contact with atmosphere.

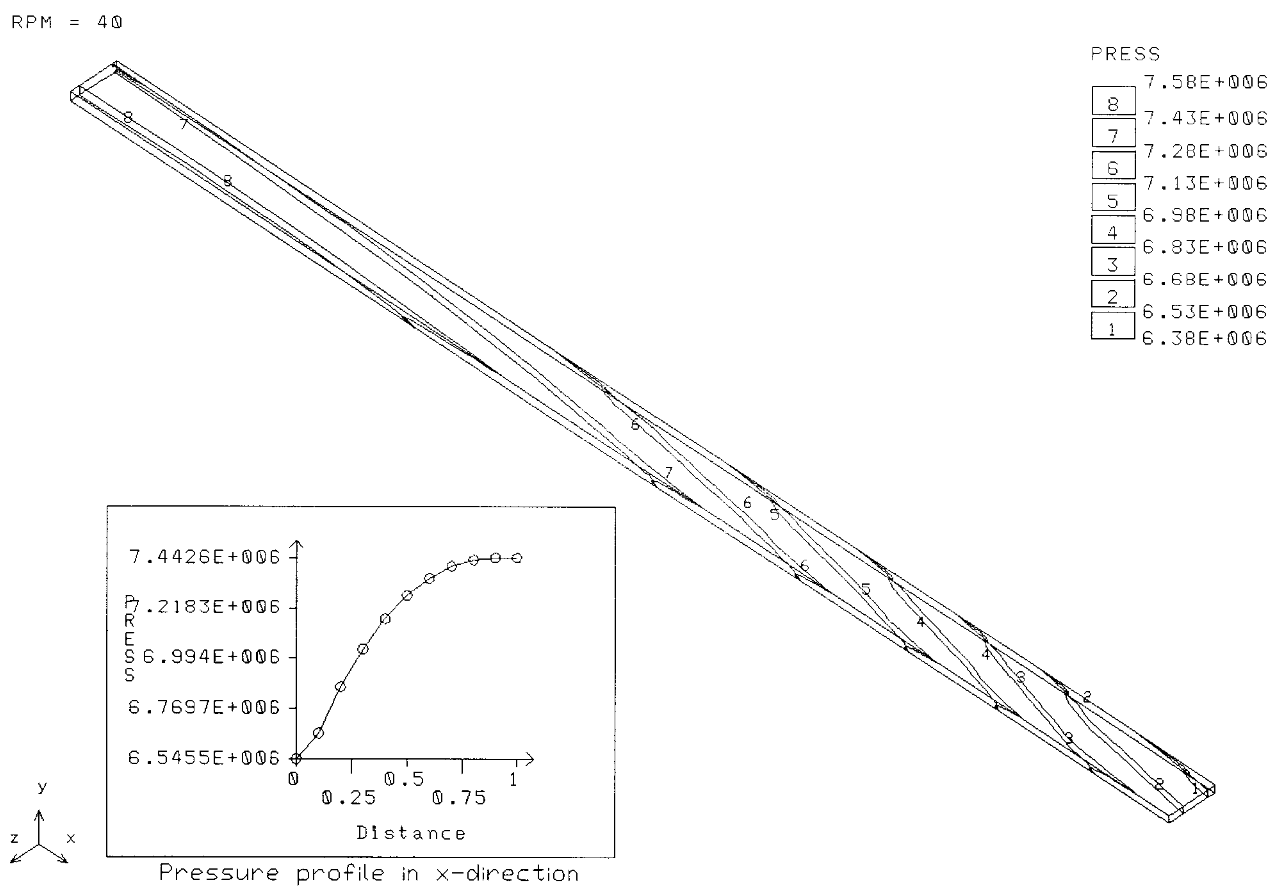

Figure 6 Pressure field in screw channel (40 rpm).

GLOBAL SOLUTION STRATEGY

Using the isoparametric mapping[20] the working equations of the present scheme are cast into a local (natural) coordinate system. The members of the coefficient matrices are then computed for each element by a Gauss quadrature method. The resulting algebraic equations are assembled into a global matrix and after imposing the appropriate set of boundary conditions are solved by a frontal solution algorithm.[22] The presence of the convective terms in the momentum and energy equations, as well as the dependency of the local viscosity on the velocity gradients and temperature, make this set of equations nonlinear. Consequently a decoupled iterative procedure based on the successive substitution method (Picard iteration method)[18] has been adopted. The first iteration starts using a set of given initial velocity and temperature values, and the coefficient matrices are computed and assembled. The global equations are then solved to obtain the velocity field. The obtained velocity field in turn is used in the calculation of viscosity and the solution of the energy equation. Using the computed velocity and temperature fields at the end of the first iteration, a new iteration step is performed. The procedure is repeated until the velocity and the temperature fields are converged. The convergence criterion used in this work is given by

$$\left(\frac{\sum_{i=1}^{N} |X_i^{r+1} - X_i^{r}|^2}{\sum_{i=1}^{N} |X_i^{r+1}|^2} \right)^{1/2} \leq \delta \tag{14}$$

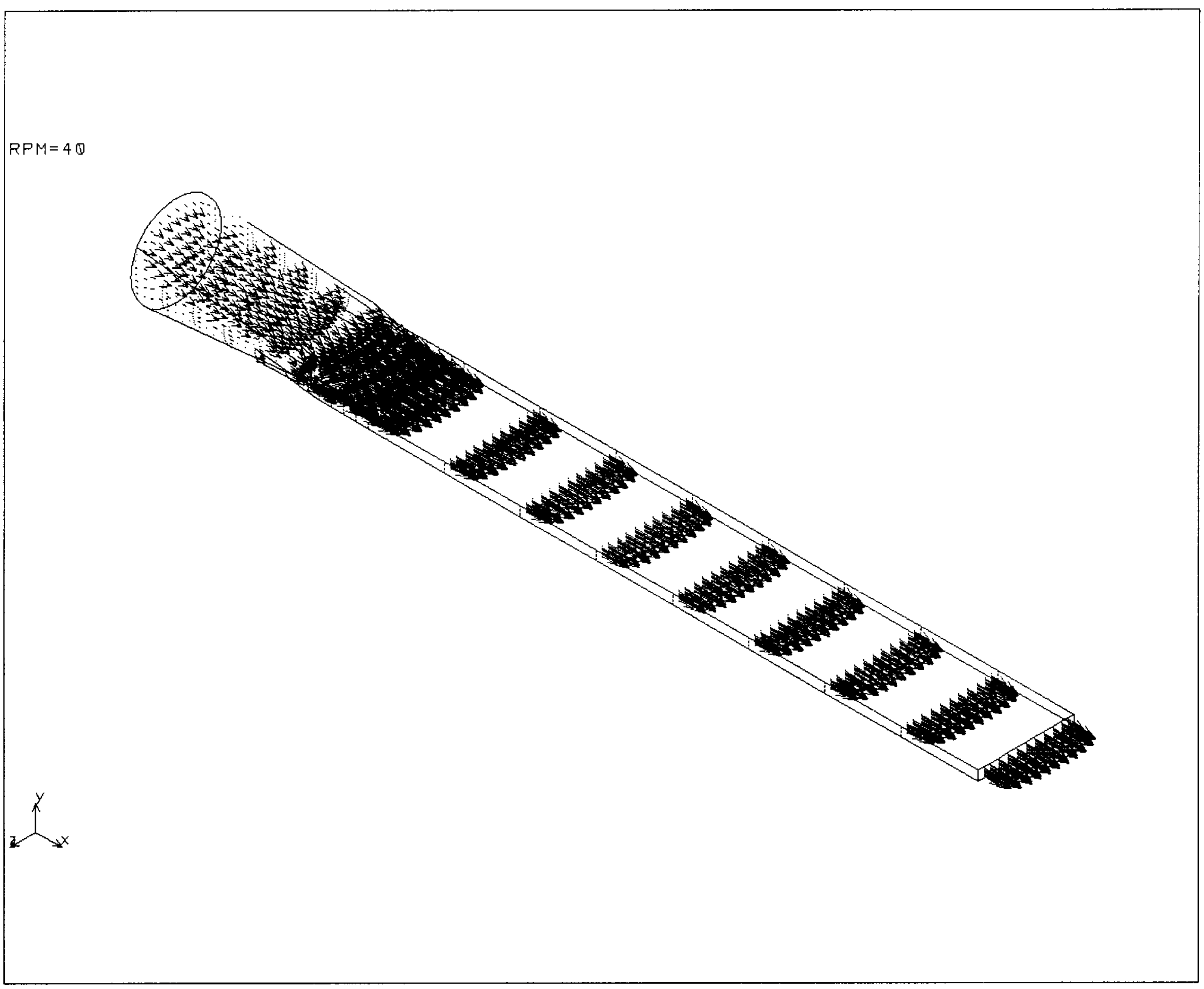

Figure 7 Velocity field in die (40 rpm).

where X_i^r denotes the flow variables (velocity or temperature) at degree of freedom i at iteration cycle of r, and δ is the convergence tolerance (say, 10^{-3}).

RESULTS AND DISCUSSION

Based on the above described computational methods, a computer code is developed in FORTRAN language. This computer program has been employed to simulate the flow of a polypropylene (T30S) melt through the metering and die regions of a single screw extruder. To verify the proposed mathematical model and the numerical algorithm, the results of the simulations are compared with the experimental runs on a laboratory extruder (Haake HBI SYS 90). Flow domains of the unrolled screw channel and die along with the boundary conditions are shown in Figures 1 and 2. The domains of the screw channel and die are divided into 1000 and 1920 eight noded Lagrangian elements with total number of nodes equal to 1331 and 2457, respectively (see Figs. 3 and 4). Trying several mesh designs, these configurations are found convergent. Pre- and postprocessing steps in the present analyses are performed using an interactive commercial package called GEOSTAR.[23] The flow of the polymer melt over the screw flight tips (leakage flow) is also taken into account based on the method presented in ref. 3. Six screw speeds (10, 20, 30, 40, 50, and 60 rpm) are selected. For each experiment, the pressure at the start of the flow into the metering zone, at the end of the metering zone or the start of the flow into the die region and two locations on the die, mass flow rate, and entrance temperature are measured (see Figs. 1 and 2). During the simulation of the flow in the screw channel, the measured pressure at the input and output sections are considered as the secondary type boundary conditions. The temperature on the solid walls and the inlet section is set to 200°C. For the analysis of the flow in die, the measured pressure and calculated temperature at the output section of the screw are considered as the input pressure and temperature to the die region. The temperature of the solid surfaces is also

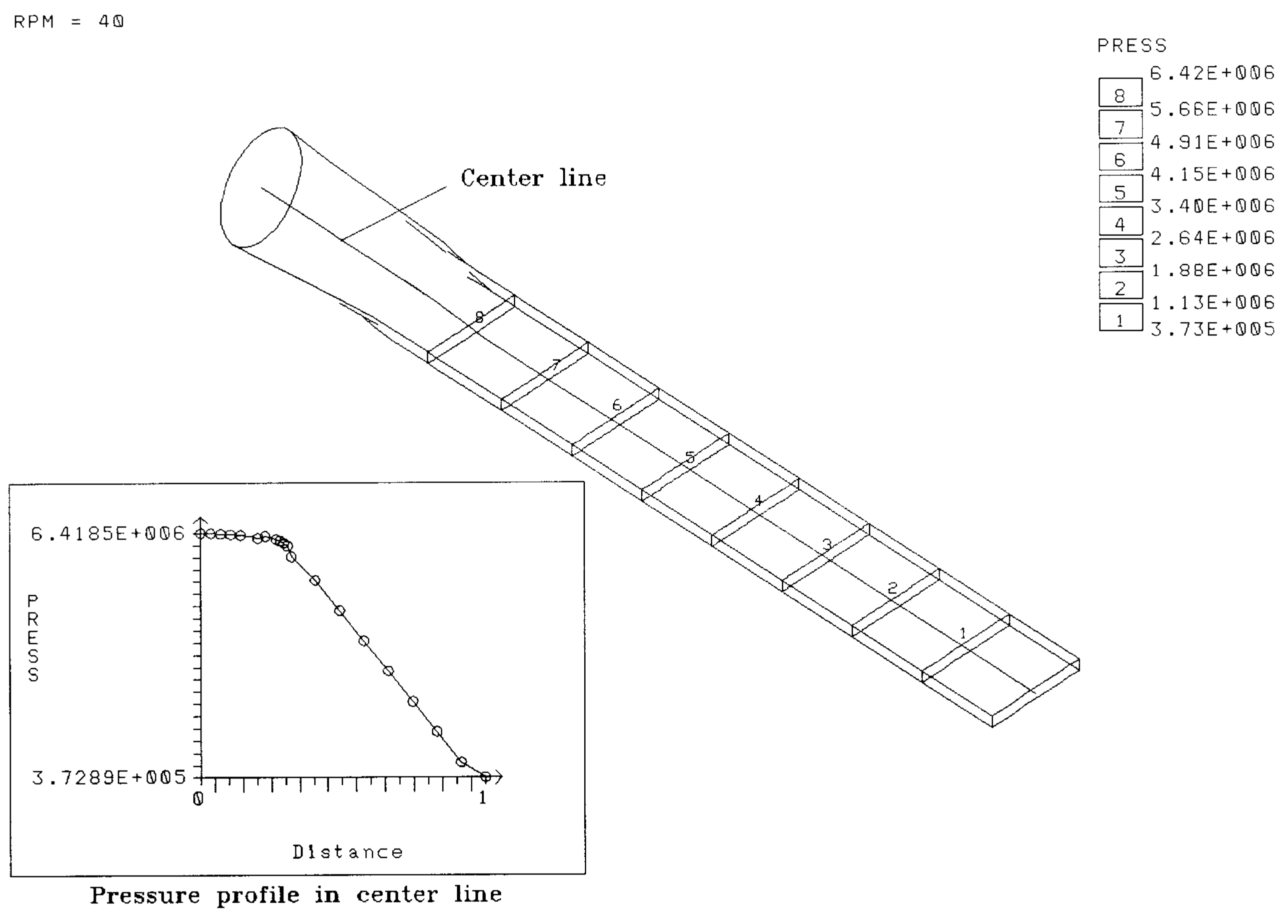

Figure 8 Pressure field in die (40 rpm).

Table III Calculated and Experimental Flow Rates in Screw Channel

Screw Speed (RPM)	Input Pressure (MPa)	Output Pressure (MPa)	Mass Flow Rate, Experimental (g/s)	Mass Flow Rate, Calculated by FEM (g/s)	Mass Flow Rate, Calculated by Fenner's Method (g/s)
10	3.8	3.03	0.105	0.105	0.115
20	5.39	4.61	0.215	0.205	0.223
30	6.78	5.69	0.321	0.311	0.338
40	7.43	6.42	0.425	0.408	0.443
50	8.27	7.13	0.525	0.511	0.554
60	8.77	7.72	0.629	0.606	0.657

set to 200°C. For both analyses (screw and die), the output mass flow rates are evaluated using the integration of the obtained velocity fields. Rheological behavior of the polypropylene melt has been studied using a capillary tube viscometer. It is found to be described by the power-law model. Tables I and II give the screw dimensions and the physical and rheological properties of the polypropylene melt used in this work.

The results of the simulation for a sample screw rotational speed of 40 RPM are presented in Figures 5–8. Figures 5a and 5b show the velocity fields in down-channel (x-axis) and cross-channel (z-axis) directions, respectively. As can be seen, the flow in the cross-channel direction (Figure 5b) corresponds to a closed-circuit flow pattern. This is as expected and is in agreement with earlier analyses.[1–3] The pressure distribution in the screw channel domain is shown in Figure 6. Due to the reduction of the channel height and also the temperature rise along the down-channel direction, a nonlinear pressure profile is obtained. Figures 7 and 8 show the velocity and pressure fields in die, respectively. Considering the geometry of the flow domain in the die and also the direction of the polymer melt flow, the calculated velocity and pressure distributions are as expected and closely correspond to each other. It can also be seen in Figure 8 that the pressure drop in the slit region is more significant than the converging section. This is mainly due to the noticeable difference between the average size of the cross-section areas of the two main parts (see Fig. 2). Temperature rise in these simulations is found to be within 2–3°C. Tables III and IV give the calculated and experimentally measured flow rates and pressure corresponding to each screw rotational speed, in screw channel and die, respectively. For the flow in the screw channel, the mass flow rates are also computed based on the method presented by Fenner in refs. 3 and 5. As it can be seen, there is very good agreement between the calculated results and actual data for the flow in both systems. Also, the comparison between the results of the simulation in the present work and those obtained based on the use of the Fenner's method confirms that the three-dimensional finite element analysis leads to more

Table IV Calculated and Experimental Mass Flow Rate and Pressure in Die

Screw Speed (rpm)	Input Pressure (MPa)	Mass Flow Rate, Experimental (g/s)	Mass Flow Rate, Calculated by FEM (g/s)	Pressure Measured at 1st Location[a] (MPa)	Pressure Measured at 2nd Location[a] (MPa)	Pressure Calculated at 1st Location (MPa)	Pressure Calculated at 2nd Location (MPa)
10	3.03	0.105	0.093	2.17	0.45	2.10	0.44
20	4.61	0.215	0.214	3.25	0.65	3.22	0.67
30	5.69	0.321	0.326	3.97	0.81	3.96	0.83
40	6.42	0.425	0.416	4.48	0.93	4.46	0.93
50	7.13	0.525	0.513	4.94	0.97	4.97	1.04
60	7.72	0.629	0.602	5.33	1.10	5.36	1.12

[a] See Figure 2.

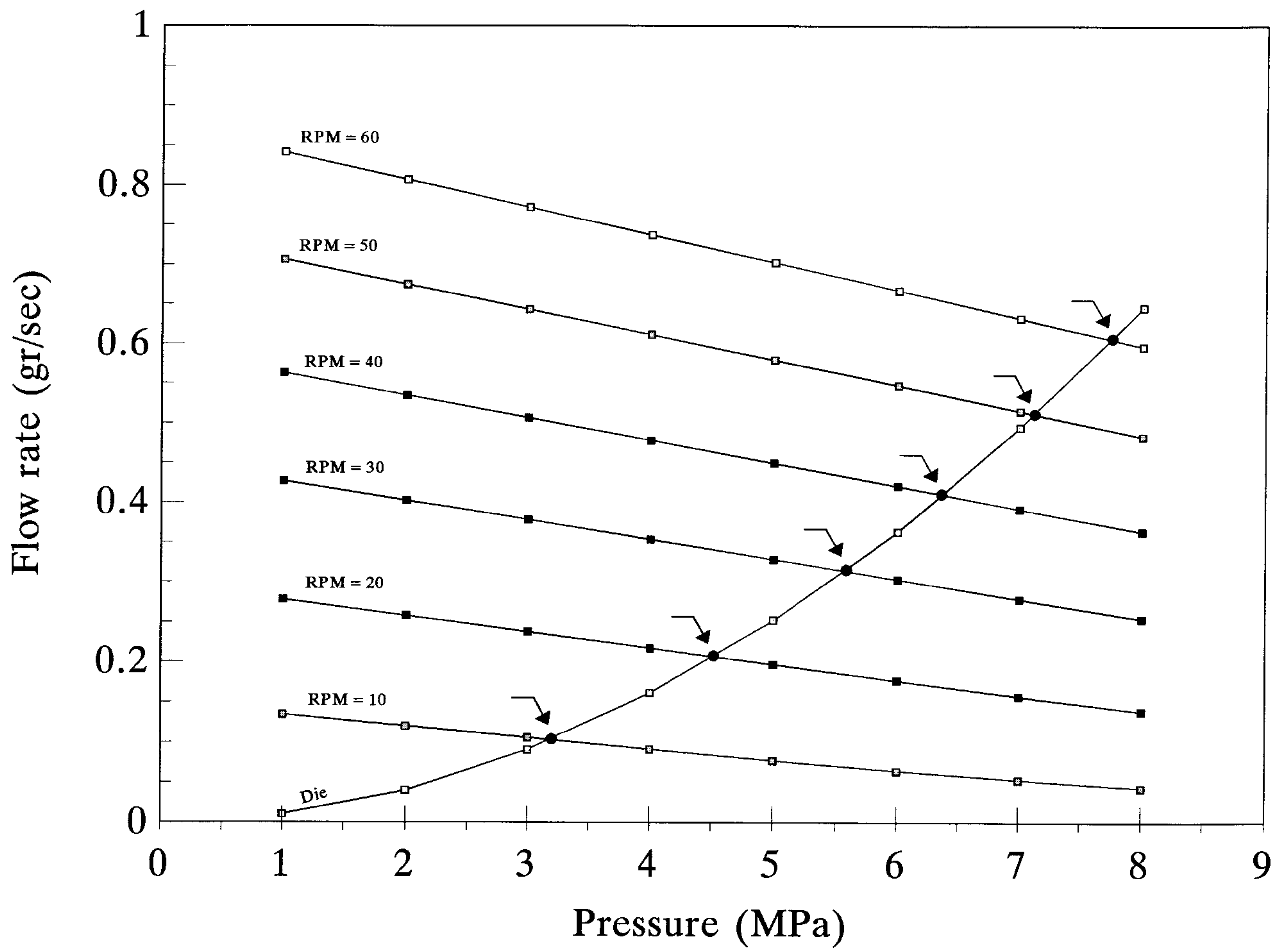

Figure 9 Characteristic curves of the screw and die with operating points.

accurate results. To determine the extruder operating points associated with each screw rotational speed, the screw and die characteristic curves are found. These curves are shown in Figure 9. The intersection between each screw characteristic curve and the characteristic curve of the die gives the extruder operating points. These points are shown in Figure 9 by six arrow symbols. Table V also gives the numerical values of the calculated operating points along with their experimentally measured values. It can be seen here that there are also very good agreements between the actual values of the operating points and the calculated ones.

Table V Calculated and Experimental Operating Points of Extruder at Various Screw Speeds

Screw Speed (RPM)	Flow Rate (g/s)		Pressure (MPa)	
	Experimental	Calculated	Experimental	Calculated
10	0.105	0.103	3.03	3.22
20	0.215	0.207	4.61	4.53
30	0.321	0.314	5.69	5.58
40	0.425	0.410	6.42	6.37
50	0.525	0.511	7.13	7.12
60	0.629	0.606	7.72	7.75

CONCLUSION

Using powerful finite element technique, we have developed a mathematical model for the three-dimensional analysis of the flow of generalized Newtonian fluids through the metering and die regions of single screw extruders. Comparisons of the numerical results and experimental measurements for the flow of a polypropylene melt show good agreement between these sets of data. Therefore, the developed model can very effectively cope with the simulation of the flow of polymeric fluids in the metering and die zones of single screw extruders and provides a straightforward and reliable method for such problems.

APPENDIX

—Flow equations,

$$\begin{bmatrix} [K^{11}] & [K^{12}] & [K^{13}] \\ [K^{21}] & [K^{22}] & [K^{23}] \\ [K^{31}] & [K^{32}] & [K^{33}] \end{bmatrix} \begin{bmatrix} \{\nu_x\} \\ \{\nu_y\} \\ \{\nu_z\} \end{bmatrix} = \begin{bmatrix} \{F^1\} \\ \{F^2\} \\ \{F^3\} \end{bmatrix} \quad (15)$$

where

$$(K^{11})_{ij} = \iiint \Big[\rho\Psi_i\Big(\bar{\nu}_x \frac{\partial \Psi_j}{\partial x} + \bar{\nu}_y \frac{\partial \Psi_j}{\partial y} + \bar{\nu}_z \frac{\partial \Psi_j}{\partial z}\Big) + \Big(2\eta \frac{\partial \Psi_i}{\partial x}\frac{\partial \Psi_j}{\partial x} + \eta \frac{\partial \Psi_i}{\partial y}\frac{\partial \Psi_j}{\partial y} + \eta \frac{\partial \Psi_i}{\partial z}\frac{\partial \Psi_j}{\partial z}\Big) + \lambda^*\Big(\frac{\partial \Psi_i}{\partial x}\frac{\partial \Psi_j}{\partial x}\Big)\Big] dx\, dy\, dz \quad (16)$$

$$(K^{12})_{ij} = \iiint \Big[\eta\Big(\frac{\partial \Psi_i}{\partial y}\frac{\partial \Psi_j}{\partial x}\Big) + \lambda^*\Big(\frac{\partial \Psi_i}{\partial x}\frac{\partial \Psi_j}{\partial y}\Big)\Big] dx\, dy\, dz \quad (17)$$

$$(K^{13})_{ij} = \iiint \Big[\eta\Big(\frac{\partial \Psi_i}{\partial z}\frac{\partial \Psi_j}{\partial x}\Big) + \lambda^*\Big(\frac{\partial \Psi_i}{\partial x}\frac{\partial \Psi_j}{\partial z}\Big)\Big] dx\, dy\, dz \quad (18)$$

$$(K^{21})_{ij} = \iiint \Big[\eta\Big(\frac{\partial \Psi_i}{\partial x}\frac{\partial \Psi_j}{\partial y}\Big) + \lambda^*\Big(\frac{\partial \Psi_i}{\partial y}\frac{\partial \Psi_j}{\partial x}\Big)\Big] dx\, dy\, dz \quad (19)$$

$$(K^{22})_{ij} = \iiint \Big[\rho\Psi_i\Big(\bar{\nu}_x \frac{\partial \Psi_j}{\partial x} + \bar{\nu}_y \frac{\partial \Psi_j}{\partial y} + \bar{\nu}_z \frac{\partial \Psi_j}{\partial z}\Big) + \Big(2\eta \frac{\partial \Psi_i}{\partial y}\frac{\partial \Psi_j}{\partial y} + \eta \frac{\partial \Psi_i}{\partial x}\frac{\partial \Psi_j}{\partial x} + \eta \frac{\partial \Psi_i}{\partial z}\frac{\partial \Psi_j}{\partial z}\Big) + \lambda^*\Big(\frac{\partial \Psi_i}{\partial y}\frac{\partial \Psi_j}{\partial y}\Big)\Big] dx\, dy\, dz \quad (20)$$

$$(K^{23})_{ij} = \iiint \Big[\eta\Big(\frac{\partial \Psi_i}{\partial z}\frac{\partial \Psi_j}{\partial y}\Big) + \lambda^*\Big(\frac{\partial \Psi_i}{\partial y}\frac{\partial \Psi_j}{\partial z}\Big)\Big] dx\, dy\, dz \quad (21)$$

$$(K^{31})_{ij} = \iiint \Big[\eta\Big(\frac{\partial \Psi_i}{\partial x}\frac{\partial \Psi_j}{\partial z}\Big) + \lambda^*\Big(\frac{\partial \Psi_i}{\partial z}\frac{\partial \Psi_j}{\partial x}\Big)\Big] dx\, dy\, dz \quad (22)$$

$$(K^{32})_{ij} = \iiint \Big[\eta\Big(\frac{\partial \Psi_i}{\partial y}\frac{\partial \Psi_j}{\partial z}\Big) + \lambda^*\Big(\frac{\partial \Psi_i}{\partial z}\frac{\partial \Psi_j}{\partial y}\Big)\Big] dx\, dy\, dz \quad (23)$$

$$(K^{33})_{ij} = \iiint \Big[\rho\Psi_i\Big(\bar{\nu}_x \frac{\partial \Psi_j}{\partial x} + \bar{\nu}_y \frac{\partial \Psi_j}{\partial y} + \bar{\nu}_z \frac{\partial \Psi_j}{\partial z}\Big) + \Big(2\eta \frac{\partial \Psi_i}{\partial z}\frac{\partial \Psi_j}{\partial z} + \eta \frac{\partial \Psi_i}{\partial y}\frac{\partial \Psi_j}{\partial y} + \eta \frac{\partial \Psi_i}{\partial x}\frac{\partial \Psi_j}{\partial x}\Big) + \lambda^*\Big(\frac{\partial \Psi_i}{\partial z}\frac{\partial \Psi_j}{\partial z}\Big)\Big] dx\, dy\, dz \quad (24)$$

and

$$(F^1)_i = \int_\Gamma \Psi_i(-pn_x + \tau_{xx}n_x + \tau_{yx}n_y + \tau_{zx}n_z)\, d\Gamma \quad (25)$$

$$(F^2)_i = \int_\Gamma \Psi_i(-pn_y + \tau_{xy}n_x + \tau_{yy}n_y + \tau_{zy}n_z)\, d\Gamma \quad (26)$$

$$(F^3)_i = \int_\Gamma \Psi_i(-pn_z + \tau_{xz}n_x + \tau_{yz}n_y + \tau_{zz}n_z)\, d\Gamma \quad (27)$$

—Energy (Heat) Equation,

$$(K_\nu)_{ij} = \iiint \left\{ \rho C_\rho \left[\Psi_i + \Phi \left(\nu_x \frac{\partial \Psi_i}{\partial x} + \nu_y \frac{\partial \Psi_i}{\partial y} + \nu_z \frac{\partial \Psi_i}{\partial z} \right) \right] \left(\nu_x \frac{\partial \Psi_j}{\partial x} + \nu_y \frac{\partial \Psi_j}{\partial y} + \nu_z \frac{\partial \Psi_j}{\partial z} \right) \right\} dx\, dy\, dz \quad (28)$$

$$(K_d)_{ij} = \iiint \left\{ k \left(\frac{\partial \Psi_i}{\partial x} \frac{\partial \Psi_j}{\partial x} + \frac{\partial \Psi_i}{\partial y} \frac{\partial \Psi_j}{\partial y} + \frac{\partial \Psi_i}{\partial z} \frac{\partial \Psi_j}{\partial z} \right) \right\} dx\, dy\, dz \quad (29)$$

$$(F_T)_i = \int_\Gamma \Psi_i \left[k \left(\frac{\partial T}{\partial x} n_x + \frac{\partial T}{\partial y} n_y + \frac{\partial T}{\partial z} n_z \right) \right] d\Gamma + \iiint \Psi_i Q\, dx\, dy\, dz \quad (30)$$

In these equations, ψ_i and ψ_j are the Lagrangian interpolation (weight) functions, respectively, Γ is the boundary of the flow domain, and n_x, n_y, and n_z are the components of the unit vector normal to the boundary in the outward direction.

REFERENCES

1. Paton, J. B.; Squires, P. H.; Darnell, W. H.; Cash, F. M. In Processing of Thermoplastic Materials; Bernhardt, E. C., Ed.; Reinhold: New York, 1960; chap 4.
2. Fenner, R. T. Extruder Screw Design; Iliffe: London, 1970.
3. Fenner, R. T. Principles of Polymer Processing; McMillan: London, 1979.
4. Agur, E. E.; Vlachopoulos, J. Polym Eng Sci 1982, 22, 1084.
5. Fenner, R. T. In Computational Analysis of Polymer Processing: Pearson, J. R., Richardson, S. M., Eds.; Applied Science: London, 1983; chap 4.
6. Elbirli, B.; Lindt, J. T. Polym Eng Sci 1984, 24, 482.
7. Steller, R. T. Polym Eng Sci 1990, 30, 400.
8. Ghoreishy, M. H. R.; Rafizadeh, M. Plastics, Rubber and Composites Processing and Applications 1996, 25, 120.
9. Fenner, R. T.; Nadiri, F. Polym Eng Sci 1979, 19, 203.
10. Mitsoulis, E. R.; Wagner, R.; Heng, F. L. Polym Eng Sci 1988, 28, 291.
11. Mahesh, G.; Kwon, T. H. Polym Eng Sci 1990, 30, 1420.
12. Karagiannis, A.; Hrymak, A. N.; Vlachopoulos, J. Rheol Acta 1990, 29, 71.
13. Coller, J. R.; Gunasekera, J. S.; Sargand, S. M. ANTEC 87 1987, 203.
14. Reese, C. ANTEC 94 1994, 94.
15. Michaeli, W. Extrusion Dies; Hanser: Munich, 1990.
16. Elbirli, B.; Lindt, J. T.; Gottgetreu, S. R.; Baba, S. M. Polym Eng Sci 1984, 24, 988.
17. Bird, R. B; Stewart, W. E.; Lighfoot, E. N. Transport Phenomena; Wiley: New York, 1960.
18. Pittman, J. F. T. In Fundamentals of Computer Modeling for Polymer Processing; Tucker, C. L., III, Ed.; Carl Hanser Verlag: New York, 1989; chap 6.
19. Ghoreishy, M. H. R.; Nassehi, V. Adv Polym Technol 1997, 16, 45.
20. Zienkiewicz, O. C.; Taylor, R. L. The Finite Element Method Vol. 1: Basic Formulation and Linear Problems, 4th ed.; McGraw-Hill: New York, 1989.
21. Brooks, A. N.; Hughes, T. J. R. Comp Meth Appl Mech Eng 1982, 32, 199.
22. Hood, P. Int J Num Meth Eng 1976, 10, 379.
23. COSMOS/M, Command Reference, Version 1.75, 1995.